



PCCP

Gas-Phase Synthesis of Corannulene – A Molecular Building Block of Fullerenes

Journal:	<i>Physical Chemistry Chemical Physics</i>
Manuscript ID	CP-ART-12-2020-006537.R1
Article Type:	Paper
Date Submitted by the Author:	05-Feb-2021
Complete List of Authors:	<p>Zhao, Long; University of Hawaii at Manoa, Department of Chemistry Doddipatla, Srinivas; University of Hawai'i at Manoa, Department of Chemistry Kaiser, Ralf; University of Hawaii, Lu, Wenchao; Lawrence Berkeley National Laboratory, Chemical Sciences Division Kostko, Oleg; Lawrence Berkeley National Laboratory, Chemical Sciences Division Ahmed, Musahid; Lawrence Berkeley National Laboratory, Chemical Sciences Division Tuli, Lotefa; Florida International University, Department of Chemistry and Biochemistry Morozov, Alexander; Florida International University Howlader, A. Hasan; Florida International University, Department of Chemistry and Biochemistry Wnuk, Stanislaw; Florida International University, Chemistry and Biochemistry Mebel, Alexander; Florida International University, Chemistry and Biochemistry Azyazov, Valeriy; Samara National Research University; Lebedev Physical Institute of RAS, Department of Chemical & Electric Discharge Lasers Mohamed, Rana; University of California Berkeley, Chemistry Fischer, Felix; University of California Berkeley, Chemistry</p>

Gas-Phase Synthesis of Corannulene – A Molecular Building Block of Fullerenes

Long Zhao, Srinivas Doddipatla, Ralf I. Kaiser*

Department of Chemistry, University of Hawaii at Manoa, Honolulu, Hawaii, 96822

Wenchao Lu, Oleg Kostko, Musahid Ahmed

*Chemical Sciences Division, Lawrence Berkeley National Laboratory, Berkeley, California
94720*

Lotefa Binta Tuli, Alexander N. Morozov, A. Hasan Howlader, Stanislaw F. Wnuk, Alexander
M. Mebel

*Department of Chemistry and Biochemistry, Florida International University, Miami, Florida
33199*

Valeriy N. Azyazov

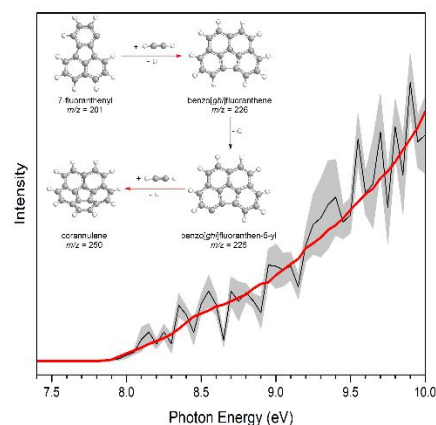
*Samara National Research University, Samara 443086 and Lebedev Physical Institute, Samara
443011, Russian Federation*

Rana K. Mohamed, Felix R. Fischer

*Department of Chemistry, University of California, Berkeley, CA 94720
Materials Sciences Division, Lawrence Berkeley National Laboratory, Berkeley, CA 94720
Kavli Energy Nano Sciences Institute at the University of California Berkeley and the Lawrence
Berkeley National Laboratory, Berkeley, California 94720*

* Corresponding author: Prof. Dr. Ralf I. Kaiser
Email: ralfk@hawaii.edu

Abstract: Fullerenes (C_{60} , C_{70}) detected in planetary nebulae and carbonaceous chondrites have been implicated to play a key role in the astrochemical evolution of the interstellar medium. However, the formation mechanism of even their simplest molecular building block — the corannulene molecule ($C_{20}H_{10}$) — has remained elusive. Here we demonstrate via a combined molecular beams and *ab initio* investigation that corannulene can be synthesized in the gas phase through the reactions of 7-fluoranthenyl ($C_{16}H_9^*$) and benzo[ghi]fluoranthen-5-yl ($C_{18}H_9^*$) radicals with acetylene (C_2H_2) mimicking conditions in carbon-rich circumstellar envelopes. This reaction sequence reveals a reaction class in which a polycyclic aromatic hydrocarbon (PAH) radical undergoes ring expansion while simultaneously forming an out-of-plane carbon backbone central to 3D nanostructures such as buckybowls and buckyballs. These fundamental reaction mechanisms are critical in facilitating an intimate understanding of the origin and evolution of the molecular universe and, in particular, of carbon in our galaxy.



Corannulene can be formed through molecular mass growth processes in circumstellar envelopes.

1. INTRODUCTION

For more than half a century, carbon-rich Asymptotic Giant Branch (AGB) stars such as IRC +10216 (CW Leonis)¹ and their descendants, planetary nebulae (PNe) like NGC 7293 (Helix Nebula),² have emerged as natural laboratories for developing our fundamental understanding of the chemical evolution of carbon-rich circumstellar envelopes (CSE).^{3, 4} The ejection of carbonaceous matter at a level of some 10^{-5} solar masses per year causes the formation of extended envelopes at temperatures of a few 1,000 K close to the central star⁵ and drive the (photochemical) synthesis of hydrogen-deficient molecules like fullerenes (C_{60} , C_{70}).⁶ A fullerene is an allotrope of carbon whose carbon atoms are arranged via fused rings of five and six atoms to form a hollow, soccer-ball (C_{60}) or ellipsoid, rugby-ball type sphere (C_{70}) (Scheme 1).⁷ These circumstellar molecules act as the molecular feedstock for carbonaceous nanoparticles (interstellar grains),⁸ which in turn have been suggested to be linked to the formation of astrobiologically relevant organics (amino acids, sugars) on their ice coated surfaces through processing by ionizing radiation.⁹ Carbonaceous organics also contribute critically to the galactic carbon budget with up to 80% of the ejected material infused into the interstellar medium.^{6, 10} However, with nearly 100 molecules detected in carbon-rich circumstellar environments, the fundamental processes involved in synthesizing the chemically most intriguing class of carbonaceous molecules - fullerenes¹¹⁻¹⁴ remain poorly explored. These pathways are critical to an understanding at the molecular level on how circumstellar envelopes — among them TC 1 as the planetary nebula toward which Buckminsterfullerene (C_{60}) was first observed via the 7.0, 8.5, 17.4, and 19.0 μm emissions¹¹ — evolve thus constraining the chemistry and the distribution of carbon in our galaxy.^{7, 12, 15-19}

In circumstellar envelopes, sophisticated *bottom-up* and *top-down* strategies have been advocated to synthesize fullerenes. Generic molecular mass growth processes incorporating often unsubstantiated gas-phase chemistries are implicated in the *bottom-up* synthesis from simple molecular building blocks involving a self-assembly of atomic carbon and dicarbon²⁰⁻²² and photochemical processing along with dehydrogenation of polycyclic aromatic hydrocarbons (PAHs) such as naphthalene in conjunction with nucleation of the C_{10} fragments.^{23, 24} The *top-down* strategy favors an ultraviolet photo processing of complex PAHs such as $C_{66}H_{20}$ ²⁴⁻²⁷ or hydrogenated amorphous carbon particles near the central star.²⁸ These pathways likely involve graphene sheets, which have been suggested to be converted to fullerenes through atomic carbon

loss accompanied by formation of five-membered rings as a prerequisite to out-of-plane bent carbon sheets. In the laboratory, solid state routes revealed the conversion of graphene to buckminsterfullerene (C_{60}) by energetic electrons²⁹ and heating of proxies of circumstellar silicon carbide nanoparticles to 1,300 K while exposing the samples to 150 keV xenon ions.³⁰ These pathways complement synthetic routes involving targeted organic precursors with predominantly existing carbon connections via flash pyrolysis of, e.g., $C_{60}H_{27}Cl_3$,³¹⁻³⁵ laser-assisted cyclodehydrogenation of $C_{60}H_{30}$,³⁵ and platinum-catalyzed cyclodehydrogenation of precursors with prevailing fullerene-type carbon skeletons such as $C_{57}H_{33}N_3$ and $C_{60}H_{30}$.^{26, 36}

It is remarkable that both the bottom-up and top-down strategies to fullerenes have faced limited efficiencies under conditions prevailing in circumstellar envelopes²⁵ with observed abundances challenging high-temperature circumstellar reaction networks derived from the chemistry of sooty environments in hydrocarbon flames.³⁷ The impending involvement of PAHs within the framework of a bottom-up^{38, 39} and top-down²⁷ synthesis of circumstellar fullerenes advocates a promising link between PAHs and fullerenes considering that these are known to coexist towards, e.g., TC 1.¹¹ However, despite this possible connection between fullerenes and PAHs, even the synthetic routes to ‘bent’ PAHs such as corannulene ($C_{20}H_{10}$) in carbon rich circumstellar envelopes are still unknown. The carbon skeleton of corannulene — the simplest representative of a circulene in which a central polygon is surrounded by and fused with benzene rings — represents the fundamental molecular building block of fullerenes and hence may signify an essential reaction intermediate in the molecular mass growth processes leading ultimately to fullerenes. This hypothesis requires the untangling of the elusive synthetic pathways to viable PAH precursors carrying an out-of-plane carbon backbone as a critical prerequisite of yielding fullerenes: corannulene ($C_{20}H_{10}$) (Scheme 1).

Here, we present a combined molecular beam and high-level *ab initio* investigation on the facile gas phase synthesis of corannulene ($C_{20}H_{10}$) in high temperature environments mimicking the conditions in carbon-rich circumstellar envelopes. The Hydrogen-Abstraction/aCetylene-Addition (HACA) and Hydrogen-Abstraction/Vinylacetylene-Addition (HAVA) mechanisms have been instrumental in elucidating the synthetic routes to the formation of planar PAHs carrying up to four fused benzene rings like triphenylene ($C_{18}H_{12}$),⁴⁰ but their validity to synthesize out-of-plane PAHs carrying a five-membered ring as present in corannulene ($C_{20}H_{10}$) has not been explored yet. Here, the gas phase synthesis of corannulene ($C_{20}H_{10}$) reveals

previously elusive chemistries of the 7-fluoranthenyl ($C_{16}H_9^{\bullet}$) and benzo[*ghi*]fluoranthen-5-yl ($C_{18}H_9^{\bullet}$) radicals with acetylene (C_2H_2) involving the HACA mechanism⁴¹ via benzo[*ghi*]fluoranthene ($C_{18}H_{10}$) intermediates through sequential bay closures accompanied by aromatization and out-of-plane bending of the carbon skeleton (Scheme 2). Corannulene represents a viable prototype intermediate and critical building block in bottom-up molecular mass growth processes from PAHs to Buckminsterfullerene (C_{60}) thus bringing us closer to an understanding of the carbon budget in our galaxy and the fundamental molecular processes of synthesizing fullerenes in circumstellar environments. Detailed experimental method and synthesis processes are provided in Supplementary Information (Supplementary Notes 1 and 2, Supplementary Schemes 1 and 2; Supplementary Figures 1–7). Briefly, a high temperature chemical reactor was used to investigate the reactions of the 7-fluoranthenyl ($C_{16}H_9^{\bullet}$) radical — generated *in situ* from 1-(2,6-dibromophenyl)naphthalene ($C_{16}H_{10}Br_2$) — with acetylene to benzo[*ghi*]fluoranthene ($C_{18}H_{10}$) and of the benzo[*ghi*]fluoranthen-5-yl radical ($C_{18}H_9^{\bullet}$) — formed *in situ* from benzo[*ghi*]fluoranthene ($C_{18}H_{10}$) — with a second acetylene molecule to corannulene ($C_{20}H_{10}$) at 1450 ± 10 K (Scheme 2). This reactor consists of a heated silicon carbide (SiC) tube and is incorporated within the source chamber of a molecular beam machine equipped with a Wiley–McLaren reflectron time-of-flight mass spectrometer (Re-TOF-MS). The reaction intermediates and products were probed isomer specifically through fragment-free photoionization in a molecular beam by tunable vacuum ultraviolet (VUV) light in tandem with the identification of the ionized molecules in a reflectron time-of-flight mass spectrometer. Mass spectra were collected by recording the arrival time of the ions as a function of mass-to-charge (m/z) ratios.

2. EXPERIMENTAL

The experiments were carried out at the Advanced Light Source (ALS) at the Chemical Dynamics Beamline (9.0.2.) utilizing a chemical reactor.⁴²⁻⁵¹ Briefly, the high temperature chemical reactor consisted of a resistively heated silicon carbide (SiC) tube of 20 mm in length and 1 mm inner diameter. In the experiment, the 7-fluoranthenyl radicals ($C_{16}H_9^{\bullet}$) were produced *in situ* at concentrations of less than 0.1 % via pyrolysis of the 1-(2,6-dibromophenyl)naphthalene ($C_{16}H_{10}Br_2$) seeded in acetylene (99.9 %; Matheson Gas) carrier gas at a pressure of 100 Torr (Supplementary Figure 4). Acetone traces in acetylene were removed by passing the acetylene gas in a cooling coil cooled through dry ice. The acetylene–1-(2,6-

dibromophenyl)naphthalene gas mixture was introduced into the silicon carbide tube (“pyrolytic reactor”) at the temperature of 1450 ± 10 K as monitored by a Type-C thermocouple. After exiting the reactor, the molecular beam, which contained the reaction products, passed through a skimmer and entered into a detection chamber, which housed the Wiley-McLaren Reflectron Time-of-Flight Mass Spectrometer (ReTOF-MS). The products were photoionized in the extraction region of the spectrometer and detected with a microchannel plate (MCP) detector. Vacuum ultraviolet (VUV) single photon ionization represents essentially a fragment-free ionization technique.⁵² Here, mass spectra were taken in 0.05 eV intervals from 7.40 eV to 10.00 eV. The photoionization efficiency (PIE) curves, which report the intensity of a specific mass-to-charge ratio (m/z) versus the photon energy, were extracted by integrating the signal collected at a well-defined m/z selected for the species of interest over the range of photon energies and normalized to the incident photon flux. The residence times of the reactants in the reactor tube (20 mm) under our experimental condition are tens of μs .⁵³⁻⁵⁵ A control experiment was also conducted by expanding neat helium carrier gas with the 1-(2,6-dibromophenyl)naphthalene ($\text{C}_{16}\text{H}_{10}\text{Br}_2$) precursor into the resistively-heated silicon carbide tube. No signal at $m/z = 226$, 227 or 250 was observed in the control experiment. 1-(2,6-Dibromophenyl)naphthalene ($\text{C}_{16}\text{H}_{10}\text{Br}_2$) was synthesized in house (Supplementary Scheme 1).

3. COMPUTATIONAL

The calculations of the energies and molecular parameters including geometries, rotational constants, and vibrational frequencies of the reactants, possible products, various intermediates and transition states for the reactions of 7-fluoranthenyl and benzo[*ghi*]fluoranthen-5-yl radicals with acetylene proceeding on the $\text{C}_{18}\text{H}_{11}$ and $\text{C}_{20}\text{H}_{11}$ potential energy surfaces (PESs), respectively, were carried out at the G3(MP2,CC)//B3LYP/6-311G(d,p) level of theory. Within this theoretical approach, geometries were optimized and vibrational frequencies were calculated using the density functional B3LYP method^{17,18} with the 6-311G(d,p) basis set. Using the optimized geometries, single-point energies were refined using a series of coupled clusters CCSD(T) and second-order Møller-Plesset perturbation theory MP2 calculations, with the final energy being computed as

$$E[\text{G3}(\text{MP2,CC})] = E[\text{CCSD}(\text{T})/6\text{-}311\text{G}(\text{d,p})] + E[\text{MP2}/\text{G3Large}] - E[\text{MP2}/6\text{-}311\text{G}(\text{d,p})] + \text{ZPE} [\text{B3LYP}/6\text{-}311\text{G}(\text{d,p})]^{19\text{-}21}$$

The G3(MP2,CC) model chemistry approach normally provides chemical accuracy of 0.01–0.02 Å for bond lengths, 1–2° for bond angles, and 3–6 kJ mol⁻¹ for relative energies of hydrocarbons, their radicals, reaction energies, and barrier heights in terms of average absolute deviations.²⁰ The adiabatic ionization energies were calculated using the same G3(MP2,CC)//B3LYP/6-311G(d,p) method with the expected accuracy of ± 0.1 eV. The GAUSSIAN 09²² and MOLPRO 2010²³ program packages were employed for the ab initio calculations.

Pressure- and temperature-dependent rate constants and product branching ratios for the 7-fluoranthenyl + C₂H₂ and benzo[ghi]fluoranthen-5-yl + C₂H₂ were evaluated using the Rice-Ramsperger-Kassel-Marcus Master Equation (RRKM-ME) theoretical approach utilizing the MESS software package.^{24,25} Densities of states and partition functions for local minima and numbers of states for transition states were computed within the Rigid-Rotor, Harmonic-Oscillator (RRHO) model. Tunneling corrections using asymmetric Eckart potentials were included in rate constant calculations. We used collision parameters for RRKM-ME calculations derived in the literature for systems of similar size; the Lennard-Jones parameters ϵ and σ for hydrocarbons were taken from Wang and Frenklach²⁶ and those for N₂ bath gas from Vishnyakov et al.^{27,28} The temperature dependence of the range parameter α for the deactivating wing of the energy transfer function was expressed as $\alpha(T) = \alpha_{300}(T/300 \text{ K})^n$, with $n = 0.62$ and $\alpha_{300} = 424 \text{ cm}^{-1}$ derived by Jasper from classical trajectory calculations²⁹ and used earlier by us in the studies of the reactions of C₂H₂ addition to various PAH radicals.³⁰⁻³² The main results of the RRKM-ME calculations of the rate constants and product branching ratios are described in Supplementary Note 2. The input files for the MESS calculations which including optimized Cartesian coordinates, vibrational frequencies, and relative energies of all species involved is provided as Supplementary Note 3.

4. RESULTS & DISCUSSION

Figure 1 displays characteristic mass spectra collected at a photoionization energy of 9.50 eV for the 1-(2,6-dibromophenyl)naphthalene (C₁₆H₁₀Br₂) precursor seeded in helium (Figure 1a) and in acetylene (Figure 1b) at a reactor temperature of 1450 ± 10 K. The 1-(2,6-dibromophenyl)naphthalene — helium system serves as a reference when compared to the 1-(2,6-dibromophenyl)naphthalene — acetylene system to unambiguously identify the m/z value(s) associated with the reaction of the radical intermediates with acetylene (Scheme 2). In the 1-(2,6-

dibromophenyl)naphthalene — helium system, signal can be observed at $m/z = 360$, 362 , and 364 . These ions can be linked to non-pyrolyzed precursor molecules: $C_{16}H_{10}^{79}Br_2$ (360 amu), $C_{16}H_{10}^{79}Br^{81}Br$ (362 amu), and $C_{16}H_{10}^{81}Br_2$ (364 amu). These precursors undergo a single carbon-bromine bond rupture yielding the 1-(1-naphthyl)-2-bromophenyl radical ($C_{16}H_{10}^{79}Br^{\bullet}$, 281 amu; $C_{16}H_{10}^{81}Br^{\bullet}$, 283 amu). Note that according to our B3LYP/6-311G** calculations, the hydrogen bromide (HBr) elimination from 1-(2,6-dibromophenyl)naphthalene is endothermic by 307 kJ mol^{-1} compared to 312 kJ mol^{-1} for the bromine atom loss, but features a barrier of 336 kJ mol^{-1} , while the atomic bromine loss occurs without an exit barrier. Thus, the atomic bromine elimination is favorable over the molecular hydrogen bromide loss both in terms of enthalpy and entropy and hence represents the dominant decomposition channel of the precursor. The 1-(1-naphthyl)-2-bromophenyl radical then undergoes a cycloaddition accompanied by atomic hydrogen loss and aromatization to 7-bromofluoranthene ($C_{16}H_9^{79}Br$, 280 amu; $C_{16}H_9^{81}Br$, 282 amu) (Supplementary Figure 8). The signal at $m/z = 280$ and 282 is clearly observable in the 1-(2,6-dibromophenyl)naphthalene–helium reference system and hence can be associated with 7-bromofluoranthene; smaller signals at a level of about $15 \pm 2\%$ are associated to $^{13}CC_{15}H_9^{79}Br$ (281 amu) and $^{13}CC_{15}H_9^{81}Br$ (283 amu). The *in situ* formed 7-bromofluoranthene can also undergo a carbon–bromine bond rupture yielding the 7-fluoranthenyl radical ($C_{16}H_9^{\bullet}$, 201 amu) which may recombine with a hydrogen atom in the reactor to fluoranthene ($C_{16}H_{10}$; 202 amu). Ion counts at $m/z = 202$ and 203 can be linked to molecules of the formulae $C_{16}H_{10}$ ($m/z = 202$) and $^{13}CC_{15}H_{10}$ ($m/z = 203$). The aforementioned ion counts are also observable in the 1-(2,6-dibromophenyl)naphthalene–acetylene system (Figure 1b) with signal at $m/z = 202$ and 203 reduced compared to the 1-(2,6-dibromophenyl)naphthalene–helium system under same counting conditions. Instead, ion counts at $m/z = 226$ and 227 dominate the mass spectrum in the 1-(2,6-dibromophenyl) naphthalene–acetylene system. Considering the mass difference of 24 amu to the reduced ion counts at $m/z = 202$ and 203 , signal at $m/z = 226$ and 227 can be connected to the product of the reaction of the 7-fluoranthenyl radical ($C_{16}H_9^{\bullet}$, 201 amu) with acetylene (C_2H_2 , 26 amu) leading to the molecules of the formulae $C_{18}H_{10}$ (226 amu) and $^{13}CC_{17}H_{10}$ (227 amu). Further molecular mass growth processes are evident from the detection of signal at $m/z = 250$ ($C_{20}H_{10}$): the $C_{18}H_{10}$ (226 amu) hydrocarbon could lose a hydrogen atom via abstraction by atomic hydrogen and/or bromine in the reactor leading to the $C_{18}H_9^{\bullet}$ radical (225 amu), which reacts with acetylene (C_2H_2 , 26 amu) to a $C_{20}H_{11}^{\bullet}$ radical intermediate (251 amu)

which is then stabilized by hydrogen atom elimination yielding a hydrocarbon with the molecular formula $C_{20}H_{10}$ (250 amu). Signal at $m/z = 304$ and 306 is observable in the 1-(2,6-dibromophenyl)-naphthalene–acetylene system, but absent in the control experiment. Considering the nearly equal intensities of both peaks and the molecular weights, these ion counts can be associated with $C_{18}H_9^{79}Br$ (304 amu) and $C_{18}H_9^{81}Br$ (306 amu) produced via the recombination of atomic bromine and the $C_{18}H_9^{\bullet}$ radical. To identify the nature of the isomers generated in these systems, photoionization efficiency (PIE) curves, which record the intensities of an ion at a well-defined mass-to-charge ratio versus the photon energy, were collected between 7.5 to 10.0 eV. The experimentally recorded PIE curves are fit with a linear combination of known PIE calibration curves of distinct structural isomers to identify which molecule(s) is(are) synthesized; the PIE calibration curves recorded in the present setup (Supplementary Figure 9).

In both the 1-(2,6-dibromophenyl)naphthalene–helium and 1-(2,6-dibromophenyl)naphthalene–acetylene systems, the PIE curves of $m/z = 360$, 362 , and 364 are superimposable after scaling and reveal an onset of the ion counts at 7.90 ± 0.05 eV. This onset correlates nicely with the computed adiabatic ionization energy of 7.85 ± 0.1 eV for the 1-(2,6-dibromophenyl)naphthalene precursor (Supplementary Figure 10). Likewise, the PIEs of $m/z = 280$ to 283 are identical within our error limits for both systems. The experimentally determined onsets of the ion counts at 7.90 ± 0.05 eV is in excellent agreement with the adiabatic ionization energy of the 7-bromofluoranthene molecule ($C_{16}H_9^{79}Br$, $C_{16}H_9^{81}Br$) of 7.88 ± 0.1 eV. Finally, the extracted PIE curves of $m/z = 202$ and 203 overlap for both systems after scaling. These graphs can be fit with the reference curve of fluoranthene ($C_{16}H_{10}$; 202 amu) along with its ^{13}C counterpart (Figure 2). At both m/z ion counts rise at 7.85 ± 0.05 eV, which correlates with the adiabatic ionization energy of fluoranthene from the reference PIE curve (7.85 ± 0.05 eV) and from literature data (7.9 ± 0.1 eV).⁵⁶ The ion counts at $m/z = 226$ ($C_{18}H_{10}$), 227 ($^{13}CC_{17}H_{10}$), and 250 ($C_{20}H_{10}$) are unique to the 1-(2,6-dibromophenyl)naphthalene–acetylene systems and hence are reaction products of the radical intermediates with acetylene. The analysis of the PIE curves underlines these findings. The PIE curves at $m/z = 226$ and 227 are superimposable after scaling and can be reproduced with a linear combination of reference PIE curves of the 7-ethynylfluoranthene and benzo[ghi]fluoranthene molecules; as revealed from the fitting procedure and visualized in Figure 2, ion counts from benzo[ghi]fluoranthene clearly dominate at a level of 96.9 ± 1.0 % at

10.0 eV. The onsets of the ion counts at 7.85 ± 0.05 eV agree well with the adiabatic ionization energy of benzo[*ghi*]fluoranthene of 7.85 ± 0.05 eV measured in this work (Supplementary Figure 9). Having established the predominant contribution of benzo[*ghi*]fluoranthene as a contributor of ion signal at $m/z = 226$ and 227 , we are analyzing the ion counts at $m/z = 250$. The corannulene reference PIE curve correlates well with the experimentally recorded PIE curve of $m/z = 250$ in the 1-(2,6-dibromophenyl)naphthalene–acetylene system. The onsets of the ion counts at 7.85 ± 0.05 eV (reference curve) and 7.85 ± 0.05 eV (experimental PIE curve) replicate well the adiabatic ionization energy of corannulene of 7.83 ± 0.02 eV,⁵⁷ respectively. Altogether, the experiments propose that in the 1-(2,6-dibromophenyl)naphthalene–acetylene system, benzo[*ghi*]fluoranthene ($C_{18}H_{10}$) and corannulene ($C_{20}H_{10}$) represent distinct reaction products, which are absent in the control experiment when acetylene is absent. On the other hand, fluoranthene ($C_{16}H_{10}$) is formed in both systems suggesting that it is the hydrogen recombination product of the reaction of 7-fluoranthenyl radical ($C_{16}H_9^*$) with atomic hydrogen in both systems.

Our experimental investigations reveal that corannulene ($C_{20}H_{10}$, 250 amu) — a prototype non-planar PAH and molecular building block of fullerenes — is synthesized via molecular mass growth processes involving reactions of the 7-fluoranthenyl radical ($C_{16}H_9^*$, 201 amu) and of the benzo[*ghi*]fluoranthen-5-yl radical ($C_{18}H_9^*$, 225 amu) with acetylene (C_2H_2 , 26 amu). To unravel the underlying reaction mechanisms, we combined these experimental findings with electronic structure calculations (Figure 3). Our computations reveal that molecular mass growth processes can account for the formation of benzo[*ghi*]fluoranthene ($C_{18}H_{10}$) (Figure 3a) and corannulene ($C_{20}H_{10}$) (Figure 3b, Supplementary Figure 11). The 7-fluoranthenyl radical ($C_{16}H_9^*$) can add with its radical center to one of the carbon atoms of the acetylene molecule via an entrance barrier of 10 kJmol^{-1} yielding a doublet radical intermediate **i1**. The latter can ring-close to **i4** by overcoming a barrier to isomerization of only 66 kJmol^{-1} . This intermediate can eliminate a hydrogen atom from the C1 position of the fluoranthene moiety yielding benzo[*ghi*]fluoranthene ($C_{18}H_{10}$) (**p1**) via a tight exit transition state in an overall exoergic reaction (-195 kJmol^{-1}). Alternatively, in a more energetically favorable pathway, a hydrogen shift from C1 of the fluoranthene unit to the terminal carbon atom of the acetylenic side chain can form intermediate **i2** which subsequently undergoes ring closure to **i3**. The latter loses atomic hydrogen accompanied by aromatization to form the planar, C_{2v} symmetric benzo [i]fluoranthene

(C₁₈H₁₀). Our computations also propose that 7-ethynylfluoranthene (**p2**) is formed via hydrogen loss from intermediate **i1**. According to RRKM-Master Equation (RRKM-ME) calculations at the conditions inside the chemical reactor, relative yields of **p1** and **p2** constitute 93% and 7%, respectively (Supplemental Note 2, Supplementary Figure 12).

The mechanism of the transformation from benzo[*ghi*]fluoranthene (C₁₈H₁₀) to corannulene (C₂₀H₁₀) mirrors the conversion from fluoranthene (C₁₆H₁₀) to benzo[*ghi*]fluoranthene (C₁₈H₁₀). This sequence is initiated by a carbon-hydrogen bond cleavage and hydrogen atom loss from benzo[*ghi*]fluoranthene (C₁₈H₁₀) to the benzo[*ghi*]fluoranthene-5-yl radical (C₁₈H₉[•]). In the chemical reactor, this might be induced by hydrogen abstraction, whereas in the circumstellar envelope, photolysis may lead to atomic hydrogen elimination. The benzo[*ghi*]fluoranthene-5-yl radical (C₁₈H₉[•]) adds then with its radical center to the acetylenic bond of acetylene passing an entrance barrier of 18 kJmol⁻¹ to access a planar, C_s symmetric doublet radical intermediate **i5**. This radical may undergo ring closure and out-of-plane bending to **i6** via a barrier of 88 kJmol⁻¹ followed by hydrogen ejection from the C10 carbon atom through a tight, C₁ symmetric transition state forming the C_{5v} symmetric corannulene (C₂₀H₁₀, **p3**) in an overall exoergic reaction (-144 kJmol⁻¹). A second, more preferable pathway to corannulene (C₂₀H₁₀) involves a hydrogen migration from the C6 atom of the benzo[*ghi*]fluoranthene moiety to the terminal carbon atom of the acetylenic side chain yielding intermediate **i7**. The latter subsequently can isomerize via ring closure and out-of-plane bending to **i8**, which ejects a hydrogen atom accompanied by bay closure and aromatization, yielding eventually corannulene (C₂₀H₁₀, **p3**). Alternatively, **i6** can also isomerize to **i8** via hydrogen migration from C10 to C1 eventually yielding corannulene through atomic hydrogen loss. The computations suggest that 5-ethynylbenzo[*ghi*]fluoranthene (C₂₀H₁₀, **p4**), might be also formed from **i5**. RRKM-ME calculated relative yields of **p3** and **p4** are 73% and 27%, respectively (Supplementary Notes 4 and 5; Supplementary Figure 13). It should be highlighted that our experiments reveal branching ratios of ion counts; due to the lack of available photoionization cross sections, branching ratios of the products cannot be estimated. Nevertheless, both the experiments and computations reveal the formation of corannulene; our computations predict that the 5-ethynylbenzo[*ghi*]fluoranthene isomer could also be a contributor, but at lower fractions than corannulene. We would like to recall that the PIE curve at m/z = 250 could be replicated by calibration curve of corannulene recorded within the same experimental setup.

5. CONCLUSIONS

The high-temperature formation of corannulene ($C_{20}H_{10}$) defines a benchmark of sequential HACA-type bay closures on armchair edges of PAH molecules involving molecular mass growth processes from *planar* PAHs (fluoranthene ($C_{16}H_{10}$), benzo[*ghi*]fluoranthene ($C_{18}H_{10}$)) to a *non-planar* PAH (corannulene ($C_{20}H_{10}$)) via 7-fluoranthenyl ($C_{16}H_9^*$) and benzo[*ghi*]fluoranthen-5-yl radicals ($C_{18}H_9^*$) (Scheme 2). In carbon rich circumstellar envelopes of Asymptotic Giant Branch stars and of planetary nebulae, the 7-fluoranthenyl ($C_{16}H_9^*$)-acetylene (C_2H_2) and benzo[*ghi*]fluoranthen-5-yl ($C_{18}H_9^*$)-acetylene (C_2H_2) reactions can be initiated through abstraction of a hydrogen atom from the 7- and 5-position of fluoranthene ($C_{16}H_{10}$) and benzo[*ghi*]fluoranthene ($C_{18}H_{10}$), respectively. The barriers for the hydrogen abstraction can be easily overcome in high temperature circumstellar environments at temperatures of a few 1,000 K.⁶ Alternatively, the strong photon field of the central star might lead to homolytic carbon-hydrogen bond rupture processes leading to 7-fluoranthenyl ($C_{16}H_9^*$) and benzo[*ghi*]fluoranthen-5-yl ($C_{18}H_9^*$) from fluoranthene ($C_{16}H_{10}$) and benzo[*ghi*]fluoranthene ($C_{18}H_{10}$), respectively. In these high temperature environments, the fluoranthene molecule ($C_{16}H_{10}$) can be easily synthesized through the Phenyl-Addition-Cyclization (PAC) mechanism⁵⁸ from 1-phenylnaphthalene ($C_{16}H_{12}$), which in turn can be formed via the elementary reaction of the phenyl radical ($C_6H_5^*$) with naphthalene ($C_{10}H_8$) (Scheme 2).⁵⁸ Note that naphthalene ($C_{10}H_8$) is accessible from the phenyl radical ($C_6H_5^*$) either via the HACA⁵¹ or HAVA pathway.⁵⁵ In carbon rich circumstellar envelopes, this bottom-up synthesis eventually leads from a single ring aromatic (phenyl ($C_6H_5^*$)) through successive molecular mass growth processes (of the reaction intermediates) involving vinylacetylene (C_4H_4), acetylene (C_2H_2) to a prototype of a non-planar PAH — corannulene ($C_{20}H_{10}$) — through highly complementary reaction mechanisms (HACA, HAVA, PAC).

The complementary nature of the PAC, HAVA, and HACA mechanisms along with their critical role in the bottom-up synthesis of non-planar PAHs (corannulene ($C_{20}H_{10}$)) is highlighted in Schemes 1 and 2. The aromatic corannulene molecule consists of a five-membered ring fused with five benzene rings and is classified as a [5]circulene. This bowl-shaped geodesic polyarene represents *the* most fundamental, buckybowl-type molecular building blocks of fullerenes and also of carbon nanotubes. The aromaticity of corannulene can be best understood in terms of the

annulene-within-an-annulene model⁵⁹ defining corannulene via a central 6π cyclopentadienyl anion surrounded by an aromatic 14 π annulenyl cation.⁶⁰ Whereas the next higher member of the circulenes — [6]circulene or coronene ($C_{24}H_{12}$) — consists of a central hexagon fused with six benzene rings and represents a central PAH intermediate to 2-dimensional carbonaceous nanostructures detected as 80 nm graphitized carbon grains in carbonaceous meteorites like Murchison and Allende,⁶¹ the [5]circulene — corannulene — defines a central molecular fragment of fullerenes (C_{60} , C_{70}) along with 3-dimensional carbonaceous nanostructures (carbon nanotubes) proposed to exist in chondrites (Scheme 1).

Previous high-temperature circumstellar reaction networks borrowed from sooty hydrocarbon flames have revealed limited efficiencies under conditions prevailing in circumstellar envelopes to synthesize fullerenes predominantly due to the lack of constrained and validated mechanisms leading to PAHs and fullerenes.^{58, 62} These high temperature reaction mechanisms in carbon rich circumstellar envelopes are similar — albeit under the exclusion of oxygen — to the bottom-up formation of PAHs probed in sooting combustion flames of, e.g., methane,⁶³ acetylene,⁶⁴ and benzene⁶⁵ revealing the ubiquitous presence of aromatics like fluoranthene, benzo[*ghi*]fluoranthene, and corannulene along with fullerenes (C_{60} , C_{70}). The reaction pathways to corannulene revealed in the present study and the potential role of corannulene in the formation of fullerenes gain strong support from sophisticated examinations of carbonaceous chondrites. Along with $^{13}C/^{12}C$ isotopic analysis, fluoranthene ($C_{16}H_{10}$),⁶⁶ benzo[*ghi*]fluoranthene ($C_{18}H_{10}$),^{66, 67} corannulene ($C_{20}H_{10}$),⁶⁷ buckminsterfullerene (C_{60}),⁶⁷⁻⁷² and rugbyballene (C_{70})^{67, 68, 71, 72} have been detected in, e.g., Murchison, Allende, Orgueil, and Tagish Lake thus corroborating impending molecular mass growth processes from fluoranthene via benzo[*ghi*]fluoranthene to corannulene and conceivably to fullerenes. It is important to point out that once PAHs form in circumstellar envelopes of carbon rich stars and are injected into the interstellar medium, they can be destroyed by photons, shocks and galactic cosmic rays envisaging lifetimes of only about 10^8 years.⁷³ However, the PAH abundance injected into the interstellar medium is in the order of 10% of the elemental carbon,⁷⁴ whereas the concentrations of PAHs in meteorites are measured only in parts per million (ppm). These considerations reveal that the absolute amount of PAHs synthesized in circumstellar envelopes and incorporated in carbonaceous chondrites is small, but nevertheless measurable. Overall, our findings establish a rigorous framework of a bottom-up synthesis of corannulene ($C_{20}H_{10}$) and provide a molecular

tracer to allow astrochemists to establish a mechanistic understanding, verified both by experiment and theory and able to explain the presence of PAHs and potentially fullerenes in deep space. These findings eventually transform the way how we think about the origin and evolution of carbonaceous matter in our galaxy.

Acknowledgments

This work was supported by the US Department of Energy, Basic Energy Sciences DE-FG02-03ER15411 (experimental studies) and DE-FG02-04ER15570 (computational studies), to the University of Hawaii and to Florida International University. W.L., O.K. and M.A. are supported by the Director, Office of Science, Office of Basic Energy Sciences, of the U.S. Department of Energy under Contract No. DE-AC02-05CH11231, through the Gas Phase Chemical Physics Program, Chemical Sciences Division. The Advanced Light Source is supported by the same contract. Theoretical calculations at Samara University were supported by the Ministry of Higher Education and Science of the Russian Federation under Grant No. 14.Y26.31.0020.

Author contributions

R.I.K. directed the overall project. R.K.M. synthesized the molecular precursor; L.Z., W.L. and O.K. carried out the experimental measurements; L.Z. performed the data analysis; L.B.T., A.N.M., V.N.A. and A.M.M. carried out the theoretical analysis; R.I.K., A.M.M., and M.A. discussed the data and supervised the project. F.R.F. supervised the synthesis of the molecular precursor. A.H.H. synthesized 7-ethynylfluoranthene and S.F.W. supervised the synthesis.

Competing financial interests

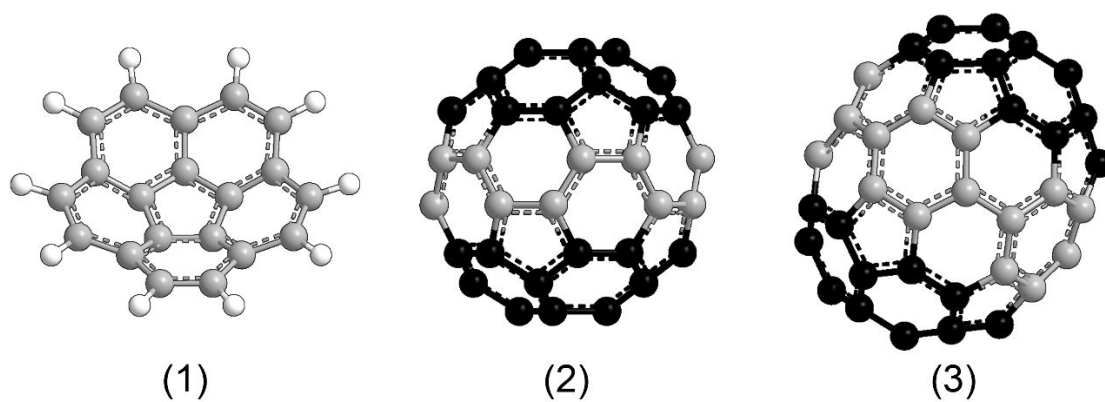
The authors declare no competing financial interests.

References

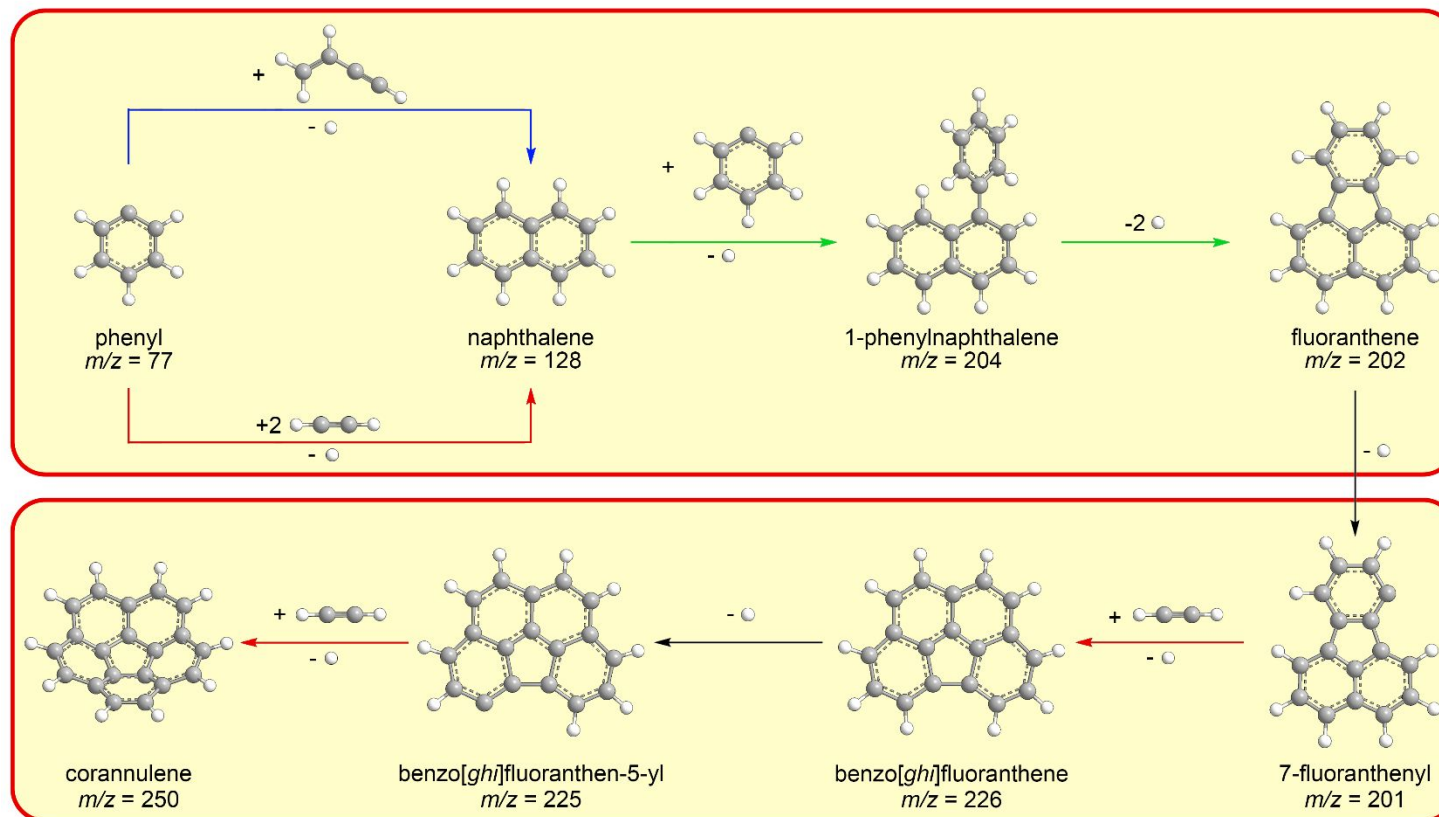
1. G. C. Clayton, D. M. Kelly, J. H. Lacy, I. R. Little-Marenin, P. A. Feldman and P. F. Bernath, *Astron. J.*, 1995, **109**, 2096-2103.
2. D. R. Schmidt, L. N. Zack and L. M. Ziurys, *Astrophys. J., Lett.*, 2018, **864**, L31/31-L31/37.
3. A. G. G. M. Tielens, *Annu. Rev. Astron. Astrophys.*, 2008, **46**, 289-337.
4. A. G. G. M. Tielens, *Rev. Mod. Phys.*, 2013, **85**, 1021-1081.
5. F. Herwig, *Annu. Rev. Astron. Astrophys.*, 2005, **43**, 435-479.
6. L. M. Ziurys, *Proc. Natl. Acad. Sci. U.S.A.*, 2006, **103**, 12274-12279.
7. H. W. Kroto, J. R. Heath, S. C. O'Brien, R. F. Curl and R. E. Smalley, *Nature*, 1985, **318**, 162-163.
8. P. Ehrenfreund and M. A. Sephton, *Faraday Discuss.*, 2006, **133**, 277-288.
9. L. J. Allamandola, *EAS Publications Series*, 2011, **46**, 305-317.
10. T. P. Snow and A. N. Witt, *Science*, 1995, **270**, 1455-1460.
11. J. Cami, J. Bernard-Salas, E. Peeters and S. E. Malek, *Science*, 2010, **329**, 1180-1182.
12. D. A. García-Hernández, S. Iglesias-Groth, J. A. Acosta-Pulido, A. Manchado, P. García-Lario, L. Stanghellini, E. Villaver, R. A. Shaw and F. Cataldo, *Astrophys. J.*, 2011, **737**, L30/31-L30/37.
13. C. Gielen, J. Cami, J. Bouwman, E. Peeters and M. Min, *A&A*, 2011, **536**, A54/51-A54/59.
14. E. Peeters, A. G. G. M. Tielens, L. J. Allamandola and M. G. Wolfire, *Astrophys. J.*, 2012, **747**, 44/41-44/11.
15. J. P. Hare, H. W. Kroto and R. Taylor, *Chem. Phys. Lett.*, 1991, **177**, 394-398.
16. D. A. García-Hernández, A. Manchado, P. García-Lario, L. Stanghellini, E. Villaver, R. A. Shaw, R. Szczerba and J. V. Perea-Calderón, *Astrophys. J.*, 2010, **724**, L39-L43.
17. K. Sellgren, M. W. Werner, J. G. Ingalls, J. D. T. Smith, T. M. Carleton and C. Joblin, *Astrophys. J.*, 2010, **722**, L54-L57.
18. Y. Zhang and S. Kwok, *Astrophys. J.*, 2011, **730**, 126/121-126/125.
19. K. R. G. Roberts, K. T. Smith and P. J. Sarre, *Mon. Not. R. Astron. Soc.*, 2012, **421**, 3277-3285.
20. P. W. Dunk, N. K. Kaiser, C. L. Hendrickson, J. P. Quinn, C. P. Ewels, Y. Nakanishi, Y. Sasaki, H. Shinohara, A. G. Marshall and H. W. Kroto, *Nat. Commun.*, 2012, **3**, 855/851 - 855/859.
21. W. Krätschmer, L. D. Lamb, K. Fostiropoulos and D. R. Huffman, *Nature*, 1990, **347**, 354-358.
22. K. Ala'a, *J. Chem. Soc., Chem. Commun.*, 1990, 1423-1425.
23. R. Taylor, G. J. Langley, H. W. Kroto and D. R. M. Walton, *Nature*, 1993, **366**, 728-731.
24. J. Zhen, P. Castellanos, D. M. Paardekooper, H. Linnartz and A. G. G. M. Tielens, *Astrophys. J.*, 2014, **797**, L30/31-L30/35.
25. O. Berne and A. G. Tielens, *Proc. Natl. Acad. Sci. U.S.A.*, 2012, **109**, 401-406.
26. G. Otero, G. Biddau, C. Sanchez-Sanchez, R. Caillard, M. F. Lopez, C. Rogero, F. J. Palomares, N. Cabello, M. A. Basanta, J. Ortega, J. Mendez, A. M. Echavarren, R. Perez, B. Gomez-Lor and J. A. Martin-Gago, *Nature*, 2008, **454**, 865-868.
27. O. Berne, J. Montillaud and C. Joblin, *A&A*, 2015, **577**, A133/131-A133/139.
28. E. R. Micelotta, A. P. Jones, J. Cami, E. Peeters, J. Bernard-Salas and G. Fanchini, *Astrophys. J.*, 2012, **761**, 35/31-35/38.
29. A. Chuvilin, U. Kaiser, E. Bichoutskaia, N. A. Besley and A. N. Khlobystov, *Nat. Chem.*, 2010, **2**, 450-453.
30. J. J. Bernal, P. Haenecour, J. Howe, T. J. Zega, S. Amari and L. M. Ziurys, *Astrophys. J.*, 2019, **883**, L43/41-L43/46.
31. L. T. Scott, M. M. Boorum, B. J. McMahon, S. Hagen, J. Mack, J. Blank, H. Wegner and A. de Meijere, *Science*, 2002, **295**, 1500-1503.
32. G. Mehta and H. S. P. Rao, *Tetrahedron*, 1998, **54**, 13325-13370.
33. M. J. Plater, M. Praveen and D. M. Schmidt, *Fullerenes, Nanotubes, and Carbon Nanostructures*, 1997, **5**, 781-800.
34. L. T. Scott, *Angew. Chem. Int. Ed.*, 2004, **43**, 4994-5007.

35. M. M. Boorum, Vasil, Y. V. ev, T. Drewello and L. T. Scott, *Science*, 2001, **294**, 828-831.
36. K. Amsharov, N. Abdurakhmanova, S. Stepanow, S. Rauschenbach, M. Jansen and K. Kern, *Angew. Chem. Int. Ed.*, 2010, **49**, 9392-9396, S9392/9391-S9392/9312.
37. H. Richter, W. J. Grieco and J. B. Howard, *Combust. Flame*, 1999, **119**, 1-22.
38. W.-W. Wang, J.-S. Dang, X. Zhao and S. Nagase, *Nanoscale*, 2017, **9**, 16742-16748.
39. J. Zhen, W. Zhang, Y. Yang, Q. Zhu and A. G. G. M. Tielens, *Astrophys. J.*, 2019, **887**, 70/71-70/79.
40. L. Zhao, B. Xu, U. Ablikim, W. Lu, M. Ahmed, M. M. Evseev, E. K. Bashkirov, V. N. Azyazov, A. H. Howlader and S. F. Wnuk, *ChemPhysChem*, 2019, **20**, 791-797.
41. M. Frenklach and E. D. Feigelson, *Astrophys. J.*, 1989, **341**, 372-384.
42. R. I. Kaiser, L. Belau, S. R. Leone, M. Ahmed, Y. M. Wang, B. J. Braams and J. M. Bowman, *Chemphyschem*, 2007, **8**, 1236-1239.
43. R. I. Kaiser, A. Mebel, O. Kostko and M. Ahmed, *Chem. Phys. Lett.*, 2010, **485**, 281-285.
44. R. I. Kaiser, B. J. Sun, H. M. Lin, A. H. H. Chang, A. M. Mebel, O. Kostko and M. Ahmed, *Astrophys. J.*, 2010, **719**, 1884-1889.
45. O. Kostko, J. Zhou, B. J. Sun, J. S. Lie, A. H. H. Chang, R. I. Kaiser and M. Ahmed, *Astrophys. J.*, 2010, **717**, 674-682.
46. F. T. Zhang, R. I. Kaiser, V. V. Kislov, A. M. Mebel, A. Golan and M. Ahmed, *J. Phys. Chem. Lett.*, 2011, **2**, 1731-1735.
47. R. I. Kaiser, S. P. Krishtal, A. M. Mebel, O. Kostko and M. Ahmed, *Astrophys. J.*, 2012, **761**, 178-184.
48. F. T. Zhang, R. I. Kaiser, A. Golan, M. Ahmed and N. Hansen, *J. Phys. Chem. A*, 2012, **116**, 3541-3546.
49. A. Golan, M. Ahmed, A. M. Mebel and R. I. Kaiser, *Phys. Chem. Chem. Phys.*, 2013, **15**, 341-347.
50. O. Kostko, B. Bandyopadhyay and M. Ahmed, *Annu. Rev. Phys. Chem.*, 2016, **67**, 19-40.
51. D. S. Parker, R. I. Kaiser, T. P. Troy and M. Ahmed, *Angew. Chem. Int. Ed.*, 2014, **53**, 7740-7744.
52. F. Qi, *Proc. Combust. Inst.*, 2013, **34**, 33-63.
53. L. Zhao, R. I. Kaiser, B. Xu, U. Ablikim, W. Lu, M. Ahmed, M. M. Evseev, E. K. Bashkirov, V. N. Azyazov, M. V. Zagidullin, A. N. Morozov, A. H. Howlader, S. F. Wnuk, A. M. Mebel, D. Joshi, G. Veber and F. R. Fischer, *Nat. Commun.*, 2019, **10**, 1510.
54. M. Zagidullin, R. Kaiser, D. Porfiriev, I. Zavershinskiy, M. Ahmed, V. Azyazov and A. Mebel, *J. Phys. Chem. A*, 2018, **122**, 8819-8827.
55. L. Zhao, R. I. Kaiser, B. Xu, U. Ablikim, M. Ahmed, M. V. Zagidullin, V. N. Azyazov, A. H. Howlader, S. F. Wnuk and A. M. Mebel, *J. Phys. Chem. Lett.*, 2018, **9**, 2620-2626.
56. Y. Ling and C. Lifshitz, *J. Phys. Chem.*, 1995, **99**, 11074-11080.
57. D. Schröder, J. Loos, H. Schwarz, R. Thissen, D. V. Preda, L. T. Scott, D. Caraiman, M. V. Frach and D. K. Böhme, *Helv. Chim. Acta*, 2001, **84**, 1625-1634.
58. L. Zhao, M. B. Prendergast, R. I. Kaiser, B. Xu, U. Ablikim, M. Ahmed, B. J. Sun, Y. L. Chen, A. H. Chang and R. K. Mohamed, *Angew. Chem. Int. Ed.*, 2019, **58**, 17442-17450.
59. E. Steiner, P. W. Fowler and L. W. Jenneskens, *Angew. Chem. Int. Ed.*, 2001, **40**, 362-366.
60. R. G. Lawton and W. E. Barth, *J. Am. Chem. Soc.*, 1971, **93**, 1730-1745.
61. L. Becker, in *Laboratory astrophysics and space research*, Springer, 1999, pp. 377-398.
62. L. Zhao, M. Prendergast, R. I. Kaiser, B. Xu, U. Ablikim, W. Lu, M. Ahmed, A. D. Oleinikov, V. N. Azyazov and A. H. Howlader, *Phys. Chem. Chem. Phys.*, 2019, **21**, 16737-16750.
63. M. J. Castaldi, A. M. Vincitore and S. M. Senkan, *Combust. Sci. Technol.*, 1995, **107**, 1-19.
64. H. Richter, E. De Hoffmann, R. Doome, A. Fonseca, J.-M. Gilles, J. B. Nagy, P. A. Thiry, J. Vandooren and P. J. Van Tiggelen, *Carbon*, 1996, **34**, 797-803.
65. W. J. Grieco, A. L. Lafleur, K. C. Swallow, H. Richter, K. Taghizadeh and J. B. Howard, *Proc. Combust. Inst.*, 1998, **27**, 1669-1675.

66. H. Naraoka, A. Shimoyama and K. Harada, *Earth Planet. Sci. Lett.*, 2000, **184**, 1-7.
67. L. Becker and T. Bunch, *Meteorit. Planet. Sci.*, 1997, **32**, 479-487.
68. M. R. Hammond and R. N. Zare, *Geochim. Cosmochim. Acta*, 2008, **72**, 5521-5529.
69. S. Pizzarello, Y. Huang, L. Becker, R. J. Poreda, R. A. Nieman, G. Cooper and M. Williams, *Science*, 2001, **293**, 2236-2239.
70. M. De Vries, K. Reihs, H. Wendt, W. Golden, H. Hunziker, R. Fleming, E. Peterson and S. Chang, *Geochim. Cosmochim. Acta*, 1993, **57**, 933-938.
71. L. Becker, J. Bada, R. Winans and T. Bunch, *Nature*, 1994, **372**, 507-507.
72. D. Heymann, *Astrophys. J. Lett.*, 1997, **489**, L111-L114.
73. E. R. Micelotta, A. P. Jones and A. G. G. M. Tielens, *A&A*, 2010, **510**, A36/31-A36/19.
74. Y. J. Pendleton and L. J. Allamandola, *Astrophys. J. Suppl. S.*, 2002, **138**, 75-98.



Scheme 1. Corannulene ($C_{20}H_{10}$, **1**) as fundamental molecular building blocks of buckminsterfullerene (C_{60} ; **2**) and rugbyballene (C_{70} ; **3**) fullerenes; the corannulene moiety is highlighted in black.



Scheme 2. Schematic representation of the formation of corannulene from the phenyl radical. Upper sequence: the bottom-up formation of fluoranthene from the phenyl radical involving three key molecular mass processes via Hydrogen-Abstraction-acetylene-Addition (HACA) (red), Hydrogen-Abstraction-Vinylacetylene-Addition (HAVA) (blue), and Phenyl-Addition-Cyclization (PAC) (green) mechanisms. Lower sequence: the formation of benzo[*ghi*]fluoranthene and corannulene through the reaction of the 7-fluoranthenyl radical ($C_{16}H_9^*$) with acetylene (C_2H_2) via HACA mechanism.

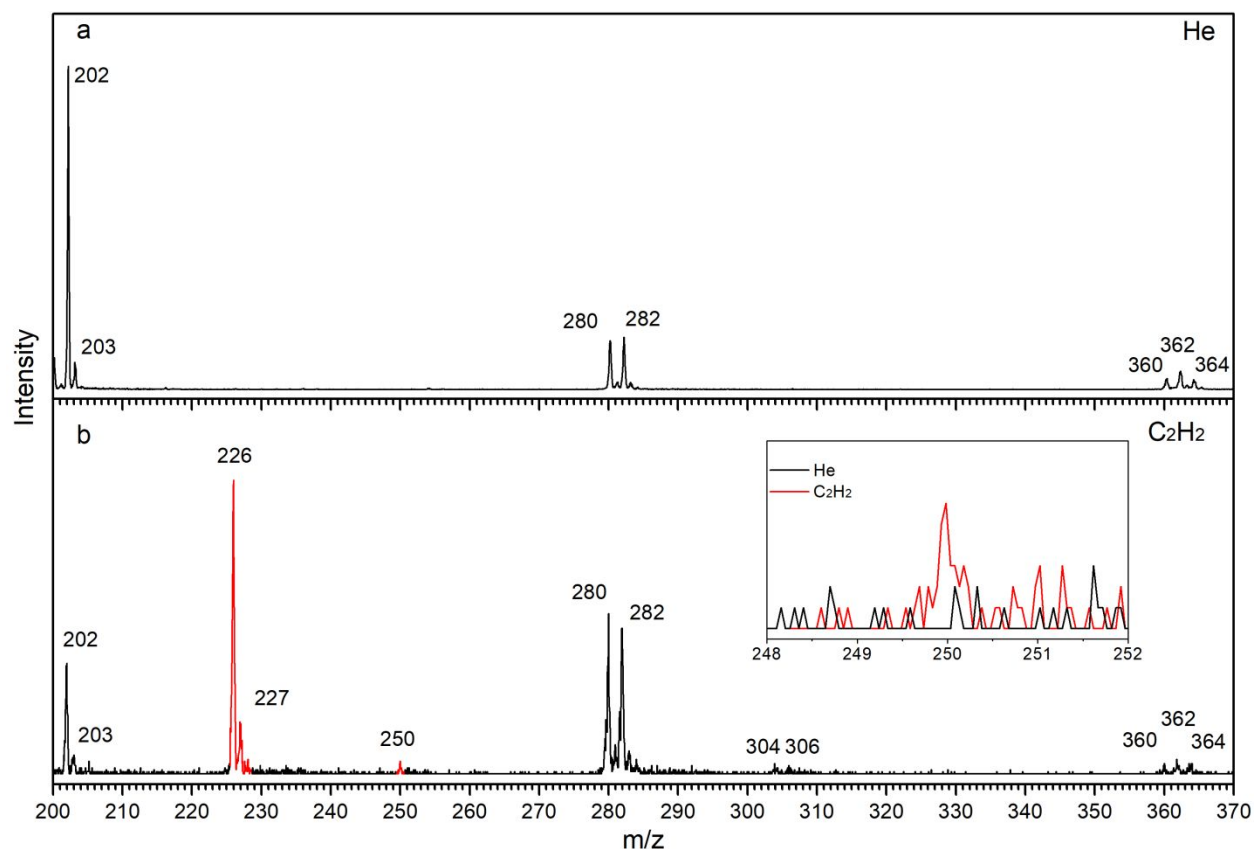


Figure 1. Photoionization mass spectra recorded at a photoionization energy of 9.5 eV at a reactor temperature of 1450 ± 10 K. (a) 1-(2,6-dibromophenyl)naphthalene ($C_{16}H_{10}Br_2$)–helium (He) system; (b) 1-(2,6-dibromophenyl)naphthalene ($C_{16}H_{10}Br_2$)–acetylene (C_2H_2) system. The mass peaks of the newly formed species at $m/z = 226$, 227 and 250 are highlighted in red. The inset shows the expanded region around $m/z = 250$.

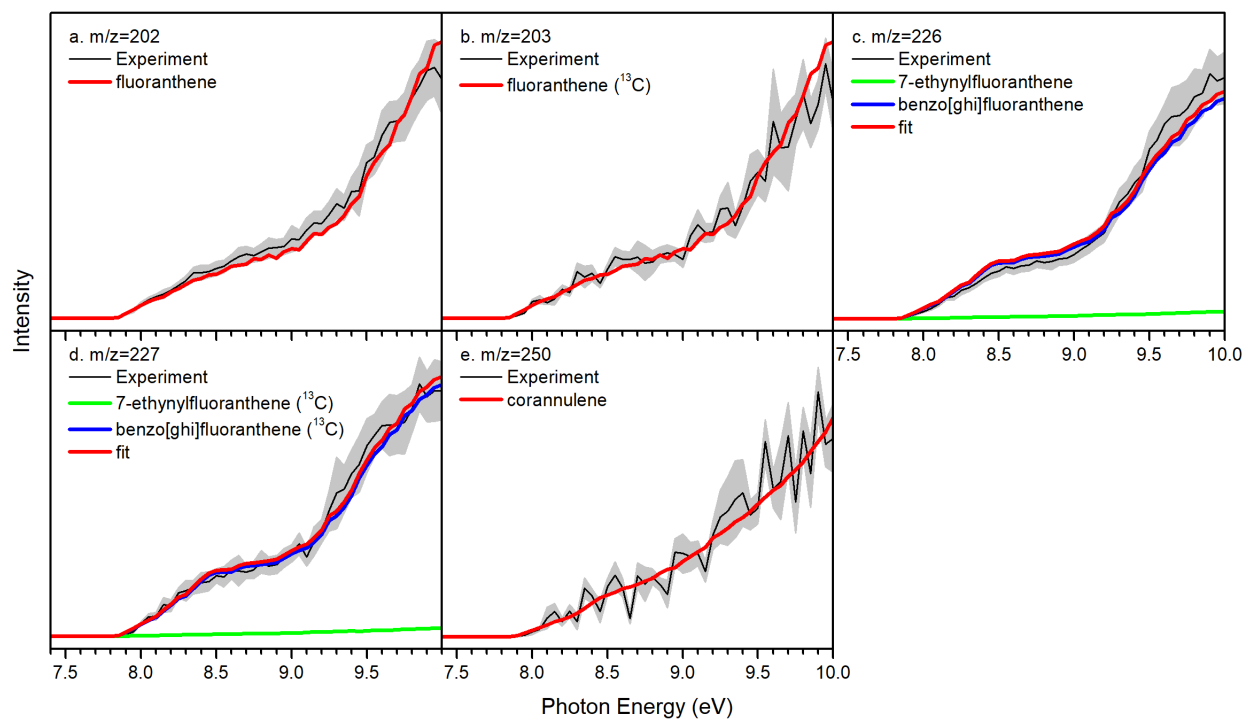


Figure 2. Photoionization efficiency (PIE) curves for $m/z = 202$, 203 , 226 , 227 and 250 . Black: experimentally derived PIE curves with the error area presented in gray; red: reference PIE curve. The overall error bars consist of two parts: $\pm 10\%$ based on the accuracy of the photodiode and a 1σ error of the PIE curve averaged over the individual scans.

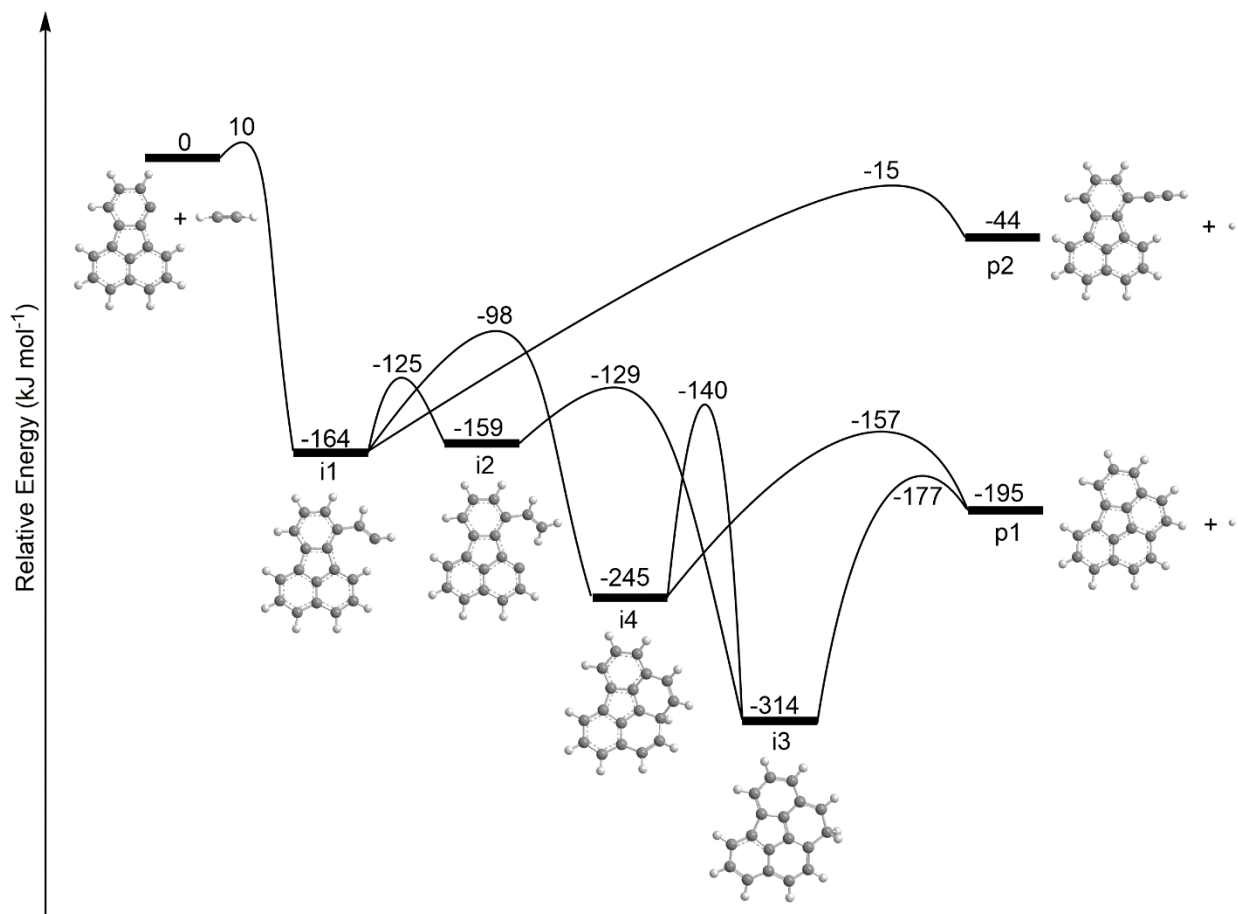


Figure 3a. Potential energy surface (PES) for the reaction of the 7-fluoranthenyl radical ($\text{C}_{16}\text{H}_9\cdot$) with acetylene (C_2H_2) calculated at the G3(MP2,CC)//B3LYP/6-311G(d,p) level of theory. The relative energies are given in kJ mol^{-1} . Cartesian coordinates of reactants, intermediates, products, and transition states are provided in the Supplementary Note 3.

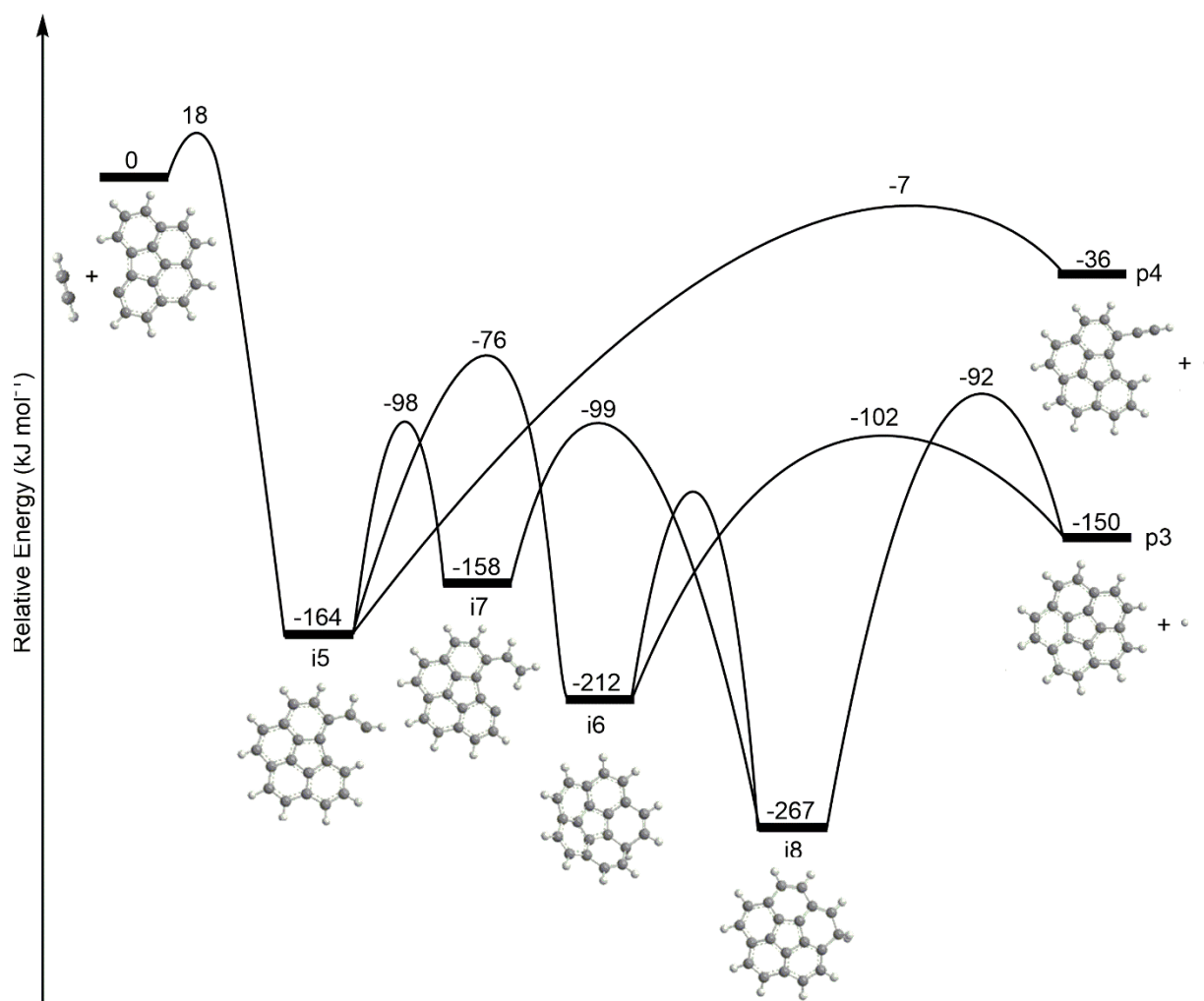


Figure 3b. Potential energy surface (PES) for the reaction of the benzofluoranthren-5-yl (C_{18}H_9) with acetylene (C_2H_2) calculated at the G3(MP2,CC)//B3LYP/6-311G(d,p) level of theory. The relative energies are given in kJ mol^{-1} . Cartesian coordinates of reactants, intermediates, products, and transition states are provided in the Supplementary Note 3.